

See discussions, stats, and author profiles for this publication at: <https://www.researchgate.net/publication/44681829>

Stable Aqueous Dispersions of Noncovalently Functionalized Graphene from Graphite and their Multifunctional High-Performance Applications

ARTICLE *in* NANO LETTERS · NOVEMBER 2010

Impact Factor: 13.59 · DOI: 10.1021/nl903557p · Source: PubMed

CITATIONS

207

READS

329

9 AUTHORS, INCLUDING:



Trevor J Simmons
Rensselaer Polytechnic Institute
31 PUBLICATIONS 623 CITATIONS

[SEE PROFILE](#)



Rakesh Shah
University of North Texas
19 PUBLICATIONS 341 CITATIONS

[SEE PROFILE](#)



Kim Michelle Lewis
Rensselaer Polytechnic Institute
35 PUBLICATIONS 268 CITATIONS

[SEE PROFILE](#)



Saroj K Nayak
Rensselaer Polytechnic Institute
178 PUBLICATIONS 3,896 CITATIONS

[SEE PROFILE](#)

Stable Aqueous Dispersions of Noncovalently Functionalized Graphene from Graphite and their Multifunctional High-Performance Applications

Xiaohong An,^{†,II} Trevor Simmons,^{†,II} Rakesh Shah,[§] Christopher Wolfe,[§] Kim M. Lewis,[†] Morris Washington,[†] Saroj K. Nayak,[†] Saikat Talapatra,[§] and Swastik Kar^{*,†}

[†]Department of Physics, Applied Physics and Astronomy and [‡]Department of Chemistry and Chemical Biology, Rensselaer Polytechnic Institute, Troy, New York 12180 and [§]Department of Physics, Southern Illinois University Carbondale, Carbondale, Illinois 62901

ABSTRACT We present a scalable and facile technique for noncovalent functionalization of graphene with 1-pyrenecarboxylic acid that exfoliates single-, few-, and multilayered graphene flakes into stable aqueous dispersions. The exfoliation mechanism is established using stringent control experiments and detailed characterization steps. Using the exfoliated graphene, we demonstrate highly sensitive and selective conductometric sensors (whose resistance rapidly changes >10 000 % in saturated ethanol vapor), and ultracapacitors with extremely high specific capacitance (~120 F/g), power density (~105 kW/kg), and energy density (~9.2 Wh/kg).

KEYWORDS Graphene, pyrenecarboxylic acid, noncovalent functionalization, aqueous dispersion, supercapacitors/ultracapacitors, sensors

Graphene, a single-atom-thick perfectly two-dimensional lattice of pure sp^2 -bonded carbon atoms has recently become a sensational material that demonstrates a number of spectacular quantum mechanical,^{1–3} optical,⁴ and molecular interaction⁵ phenomena. Most of these experiments use graphene fabricated by a “micromechanical cleavage” of graphite,^{6,7} which appears to produce graphene of the highest quality with exceptional electronic,⁸ structural,⁹ and thermal¹⁰ properties. Despite producing such high-quality graphene that is extremely useful for fundamental experiments, the micromechanical cleavage method is unsuitable for producing large quantities of graphene directly from graphite that could benefit a number of advanced large-scale applications. Most of the large-scale graphene-based applications demonstrated so far, such as transparent conductive electrodes,¹¹ gas sensors¹² and ultracapacitors,¹³ use a suspension or colloidal dispersion of different variants of chemically modified graphene or reduced graphene oxide (rGO).¹⁴ These typically involve use of strong acids and oxidants (that largely disrupt the sp^2 -bonded carbon network of graphene by forming covalently attached hydroxyl and epoxide groups), hydrazine-based reducing agents, and high temperatures. Additionally, Raman studies indicate that rGO is extremely defective^{11,15}

compared to the high quality of graphene cleaved directly from graphite.^{16–18} Hence, a simple method for large-scale production of graphene directly from graphite (that retains its high quality) is extremely desirable. Additionally, if the exfoliated graphene is dispersed in a convenient medium, it would pave the way for a number of direct application developments.

Simmons et al. have recently developed¹⁹ stable aqueous dispersions of single-wall carbon nanotubes (SWNTs) by a noncovalent functionalization of the nanotube sidewalls with 1-pyrenecarboxylic acid (PCA). The carboxylic acid group ($-COOH$) that facilitates the SWNT stability in water functionalizes the sidewalls via a nondestructive $\pi-\pi$ stacking mechanism (aromatic interaction). This stands in sharp contrast to previous reports of functionalization of carbon nanotubes that employ harsh chemical processing such as oxidative acid treatment and other covalent strategies,^{20–24} which result in significant damage of the nanotubes. Building upon this idea, in this work we describe a simple and elegant method for large-scale direct exfoliation of graphite into aqueous dispersions of single-, few-, and multilayered graphene flakes that retain their high quality.²⁵ The exfoliation has been achieved by a noncovalent functionalization of graphene with PCA in a polarity-controlled combination of media. It is well-known that the hydrophobic nature of graphitic materials coupled with the relatively stable interlayer adhesion of graphite make it difficult to directly exfoliate graphene in water. In a controlled medium, PCA overcomes this difficulty by serving a dual purpose: initially as a “molecular wedge” that cleaves the individual graphene

* To whom correspondence should be addressed. E-mail: kars@rpi.edu. Phone: 1-518-276-6410. Fax: 1-518-276-2990.

II These authors contributed equally to this work.

Received for review: 10/23/2009

Published on Web: 06/17/2010

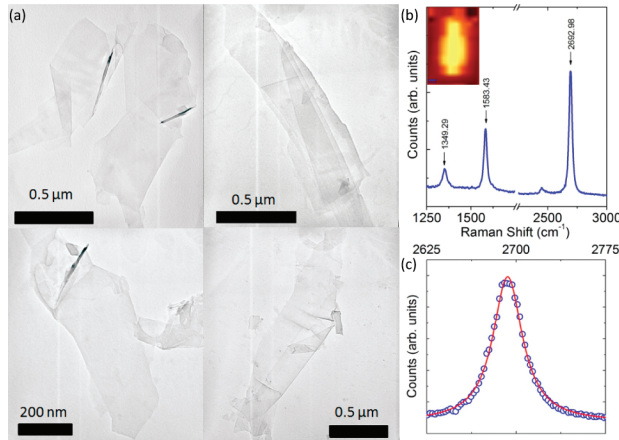


FIGURE 1. (a) TEM images of graphene flakes showing typical size, shape, and morphology of the graphene flakes obtained by our proposed “molecular wedging” of graphite. (b) Raman spectrum of a single-layer graphene flake with the G-band around 1583 cm^{-1} , corresponding to the zone center E_{2g} phonon (in-plane optical mode) of sp^2 hybridized carbon close to the Γ point. Other peaks, observed at around 1349 cm^{-1} correspond to the D-peak or the first order edge or defect-induced zone boundary phonons, and 2693 cm^{-1} (the D'-band or second-order zone boundary phonons). As seen here, the Raman spectrum of single-layer graphene has at least two unique signatures (see text). First, the D'-band peak intensity is larger than the G peak (a feature that reverses itself in graphene with number of layers >1 and in graphite). Second, the D'-band peak can be fitted with a single Lorentzian function, which is not the case of graphitic flakes with a higher number of layers, where two or more Lorentzian functions are required to fit the Raman data. (c) The single Lorentzian fit to the D'-band peak. The inset in (b) shows the spatial Raman map (image width $\sim 1.5\text{ }\mu\text{m}$) of the graphene flake obtained from the integrated D'- peak.

flakes from the parent graphite pieces, and then by forming stable polar functional groups on the graphene surface via a noncovalent $\pi-\pi$ stacking mechanism that does not disrupt its sp^2 hybridization. The hydrophilic $-\text{COOH}$ group of PCA facilitates the formation of stable aqueous dispersions of graphene, in a manner similar to that of graphene oxide, but without degrading the sp^2 structure. The physicochemical process leading to this novel exfoliation mechanism has been examined in detail with the help of stringent control experiments, and characterization using TEM (including HRTEM and SAED), SEM, AFM, Raman spectroscopy, UV-vis absorbance spectroscopy, suspension-stability investigations, and low-temperature electrical transport measurements. To demonstrate their direct usage for advanced applications, we have developed conductometric chemical sensors that can easily identify ethanol from within a mixture of gases/vapors, allowing them to be used as possible industrial leakage detectors or breath-alcohol analyzers. We also make use of the large specific surface area of graphene to build ultrathin energy-storage devices in the form of electrochemical double-layer capacitors with extremely high specific capacitance, energy density, and power densities, far superior than most past reports on similar devices built using graphitic carbon materials.

Figure 1a shows transmission electron microscope (TEM) images of typical graphene flakes transferred onto a carbon-

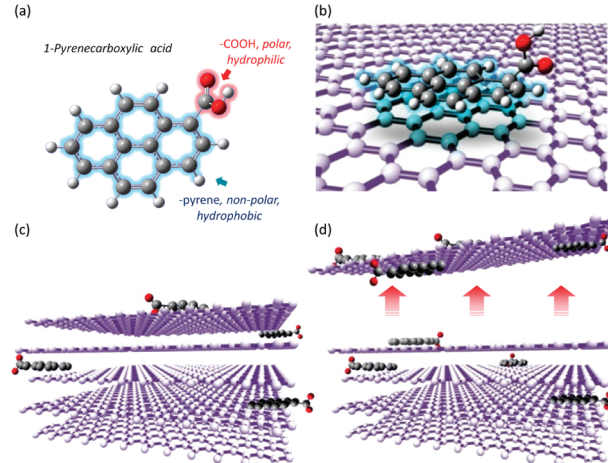


FIGURE 2. (a) Molecular structure of 1-pyrenecarboxylic acid with its polar (hydrophilic) and nonpolar (hydrophobic) parts indicated. (b) A PCA molecule can form a stable π -stacking bond with graphitic surfaces. (c) In a polar medium (H_2O) and with agitation, the nonpolar pyrene part prefers to attach itself on top of the graphitic surface via the π -stacking mechanism, or penetrates within the layers of graphite to reduce hydrophobic interactions with water. With continuous agitation, more of such molecules enter in between the layers and move in deeper, breaking the π -bonding of the intergraphene layers of the graphite. (d) Continuing this process releases single or few layers of graphene. The $-\text{COOH}$ groups of the PCA molecules (attached to the released graphene flakes) prefer the polar medium and keep the graphene flakes stably suspended in water.

film TEM grid. The presence of monolayer graphene flakes could be confirmed by transferring similar flakes onto SiO_2/Si substrates²⁵ and measuring their Raman spectra. Figure 1b shows the Raman spectrum of a typical monolayer graphene flake. The single-Lorentzian shape (Figure 1c) of the second-order zone-boundary phonon peak (at 2693 cm^{-1}) and its higher intensity compared to the G-peak (at 1583 cm^{-1}) confirm^{16,17} the monolayer nature of the graphene. AFM step-height of monolayer graphene was found to be about 0.7 nm ,²⁵ similar to previous reports.^{6,26} AFM height measurements were also used to obtain the statistics of the number of layers per flake,²⁵ from which we find that monolayers comprise of slightly less than 10 % of the graphene flakes.

The exfoliation of the graphene sheets from parent graphite pieces is the outcome of three key aspects, namely (a) the amphiphilic nature of PCA, (b) the presence of water and methanol, which play distinct roles in the exfoliation process, and (c) the agitation and precipitation steps. The mechanisms at work behind each of the steps merit examination. In the first step, PCA is mixed uniformly with methanol. PCA is a polyaromatic hydrocarbon derivative that has a polar (hydrophilic) carboxylic acid group and a nonpolar (hydrophobic) pyrene group (i.e., it has an amphiphilic nature, see Figure 2a). Methanol has a similar amphiphilic nature with a polar alcohol $-\text{OH}$ group attached to a much less polar $-\text{CH}_3$ group (dipole moment = $1.70 \pm 0.02\text{ D}$).²⁷ This enables PCA to dissolve completely into

molecular entities in methanol. When graphite powder is introduced into the PCA-methanol solution, PCA is able to interact with the exposed graphitic surface. The nonpolar pyrene portion of PCA has a fully conjugated π -network, meaning it has a continuous alternating pattern of single and double bonds and is fully aromatic, surrounded by a cloud of delocalized π -electrons. Graphene is considered to be an infinite alternant of polyaromatic hydrocarbons and is therefore also fully aromatic. The hydrophobic pyrene group of PCA has a nearly identical structure to graphene, and this allows for a strong $\pi-\pi$ stacking interaction, also known as an aromatic interaction. The interaction of the π -clouds above and below the $x-y$ plane of PCA and graphene causes $\pi-\pi$ stacking (as shown schematically in Figure 2b), an interaction stronger than other noncovalent interactions such as van der Waals forces. In this way, the top, bottom, and other exposed graphene layers of the parent graphite piece get pyrene-functionalized with dangling polar $-COOH$ groups (which find the polar methanol medium favorable). This idea has been successfully applied to debundle single wall carbon nanotubes into stable aqueous dispersions.¹⁹ Such debundling occurred due to the affinity of the hydrophobic pyrene group of PCA toward the hydrophobic surface of carbon nanotubes, which was stabilized by a (noncovalent) strong $\pi-\pi$ stacking interaction. Meanwhile the hydrophilic carboxylic acid group enabled the carbon nanotubes to be readily dispersed in water as a complex. Structurally, graphene is essentially an unrolled carbon nanotube. However, since graphite is also hydrophobic and is strongly bound by a robust interlayer interaction, the presence of the aromatic pyrene and the polar $-COOH$ group in a polar medium alone is not sufficient to dislodge the graphene flakes and bring them into the solvent medium. When this system is mixed with water, which is a more polar medium (dipole moment = 1.8546 ± 0.0040 D),²⁷ and agitated in a small bath-type sonicator, two important steps take place. First, the PCA that was stable in pure methanol is now exposed to an increasingly polar medium when water is added, and this causes the nonpolar pyrene group to become increasingly less soluble. Second, the agitation helps to open up small gaps between the edges of the graphene flakes. The amphiphilic PCA molecules, attempting to minimize their hydrophobic interactions with water, form a larger number of $\pi-\pi$ functionalized groups on the surface of graphite and also find their way to the gaps opening up at the edges, as demonstrated schematically in Figure 2c. In effect, PCA molecules form “molecular wedges” that get driven deeper and deeper into the graphitic layers with continuing agitation. The out-of-plane $-COOH$ of the inserted PCA helps to separate the graphitic layers and prevent them from reforming the $\pi-\pi$ stacking that otherwise tightly binds graphene sheets as monolithic graphite. This step is conceptually similar to the various techniques for expanding graphite via oxidative intercalation such as Hummers method.^{28–31} Eventually, with sufficient agitation, a large number of these

“molecular wedges” can enter between the graphitic layers, and separate single, double, or few-layer graphene flakes as shown in Figure 2d. After exfoliation, the same PCA molecules that performed the “molecular wedging”, now have their pyrene groups physisorbed via $\pi-\pi$ stacking interactions with the exfoliated graphene sheets. At the same time, the out-of-plane dangling hydrophilic $-COOH$ groups allow the graphene-PCA complex to remain stably suspended in water. Hence, each constituent of the process plays distinct roles. PCA acts as the molecular wedge that cleaves graphite powder to produce graphene, and functionalizes the graphene to allow stable dispersion in water. Methanol serves to dissolve as-received PCA powder completely into molecular entities at the initial stage. Graphite powder ultimately provides the graphene sheets, and water forces PCA to intercalate (and facilitated by the agitation, drives these wedges deeper) into graphite and subsequently provides a polar medium for stable graphene dispersion.

To verify our proposed concept, control experiments were performed along with our present method by attempting to produce stable aqueous dispersions of graphene (stage 3 of the process²⁵) while one or more constituent(s) were intentionally suppressed. Four possible combinations were tested, that is, sample A starting with graphite powder + water, sample B with graphite powder + PCA + water, sample C with graphite powder + PCA + methanol, and sample D with graphite powder + PCA + methanol + water (present method). First, the comparative stability of each of these combinations at stage 3 was investigated. Figure 3a visually compares the stability of these stage 3 solutions A–C against D, which represents our present method. Vials containing A–D were allowed to stand. After ten days, the graphitic material in vials A–C almost completely precipitated into a black powder at the bottom. In the case of A and C, a clear solution remained on top, while in the case of B, undissolved PCA remained suspended in water rendering it a dirty gray hue. The original solution D, however, retained its purplish gray color with almost no precipitation. This control experiment clearly establishes that each of the constituents, PCA, methanol, and water, play distinct roles in bringing about a stable final product.

Second, the final composition was analyzed after three washing steps were completed on the samples A–D and the resultant solutions were transferred onto TEM grids to further elucidate the individual roles of PCA, methanol, and water. Figure 3b shows typical examples of TEM images from the washed solutions A–D. In A and B, we found a majority of micrometer-scale graphite pieces (as a result of the sonication step) with little or no sign of even thick layers of graphene. This indicates that merely agitation or the presence of PCA is insufficient to exfoliate graphite. Owing to a relatively lower affinity of PCA for water in comparison to methanol, PCA does not dissolve sufficiently in water to a molecular level, which is important for the “wedging” mechanism to initiate. In C, similar micrometer-scale

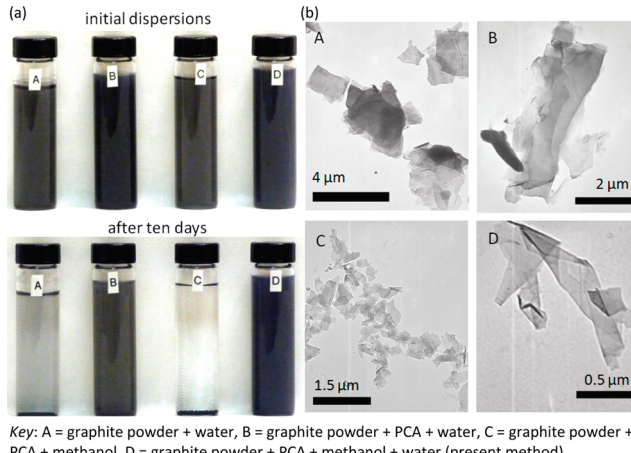


FIGURE 3. (a) Comparative stability of the dispersions at stage 3 (of Supporting Information Figure S1²⁵) with different starting ingredients (as indicated by the key). Only in case of the present method (D), the resulting dispersion is stable without significant precipitation. The dirty gray color of B after ten days is due to suspended PCA in water and hides the dark sedimentation at the bottom. (b) Typical TEM images of resultant material after three washes of the stage 3 dispersions A–D. A and B shows only presence of micrometer-scale broken graphite pieces resulting from the ultrasonication steps. The PCA present in B is unable to exfoliate graphite since it does not dissolve well (into molecular entities) in water and simply adheres to the broken graphite surfaces. C shows limited exfoliation of graphite into small pieces of multilayered graphene (possibly exfoliated during the washing stages). This process is inefficient and the resultant pieces reagglomerate as seen here. D shows a typical graphene flake similar to those shown in Figure 1. This establishes the importance of each of the starting constituents in the final formation of stably dispersed graphene in water.

graphite pieces were accompanied by some agglomerated multilayered graphene pieces. This indicates that in sample C, which contained no water, the exfoliation is inefficient since due to the lack of hydrophobic interactions, the PCA molecules are not driven into the graphitic layers, and afterward, its affinity toward methanol prevents it from forming sufficient amounts of π -stacking functionalizations to keep the multilayered graphene pieces stably dispersed. The few pieces of multilayered graphene seen in TEM images could also have been produced during the washing steps. Only in the case of D, we found large quantities of stable graphene flakes all over the TEM grid. In general, the presence of PCA exfoliates the graphite to some extent, but only through a combination of the correct media large quantities of stably dispersed graphene could be obtained.

Finally, to establish that the final graphene flakes were indeed PCA functionalized, we measured the absorption spectrum of sample D followed by washing it up to four times²⁵ (we call the first wash E, the second wash F, etc., see Figure 4). At each stage, the digital photographs of samples D–G in vials and TEM images of the composition of D–F were also taken. Figure 4 shows the relative absorbance of sample D and its washed remains E–H within the UV–visible window (250–500 nm, using a Perkin-Elmer λ -900 UV-vis-NIR spectrophotometer). PCA belongs to a large class of pyrene-based fluorophores that exhibit strong

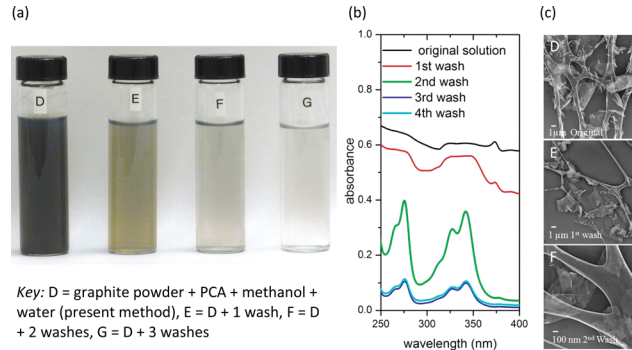


FIGURE 4. (a) Comparative appearance of the original graphene dispersion D and after each wash step (E, F, and G). (b) Absorption spectra of D and up to its four washes in the UV region. The broad absorption bands in D and E are due to the presence of large quantities of graphene (single, few, and multilayered) that renders the dispersion significantly opaque. The TEM images (c) at these stages show crystallites of PCA along with graphene. After the second wash (F), absorption peaks for PCA become clearly distinguishable, though hardly any PCA crystallites are visible in the corresponding TEM image. After the third wash (G), the extra PCA is insignificant in quantity. The absorption spectra remain practically unchanged after this wash with the peaks appearing only from the PCA molecules functionalizing on the suspended graphene flakes.

absorbance peaks even at trace amounts. Figure 4a shows the comparative appearance of the original graphene dispersion D and after each wash (E, F, and G). Figure 4b is the absorption spectrum of D–G in the UV region. The broad absorption bands in D and E are due to the presence of large quantities of graphene (single, few, and multilayered) that renders the dispersion significantly opaque. The TEM images on the right at these stages show crystallites of PCA along with graphene. After the second wash (F), absorption peaks for PCA become clearly distinguishable, though hardly any PCA crystallites are visible in the corresponding TEM image. After the third wash (G), the excess PCA is insignificant in quantity. The absorption spectra remain practically unchanged after this wash (as seen from the similarity between third and fourth wash) with the peaks appearing only from the PCA molecules functionalizing on the suspended graphene flakes.

To demonstrate the multifunctionality of the graphene flakes in a variety of large-scale applications, graphene suspensions were simply vacuum-filtered through nanoporous membranes leaving thin graphene films on the membrane²⁵ that could be used directly as chemical sensors and ultracapacitors. The conductance of graphene-based devices has been shown to be ultrasensitive to adsorbed analytes, enabling even single-molecule detection.⁵ However, this sensitivity has recently been attributed²⁶ to the presence of a monolayer of “resist” that remains after lithographic steps for attaching electrical contacts to graphene are performed. This acts as a “functionalization” layer that facilitates analyte adhesion and the consequent charge transfer (p-type or n-type doping) that leads to a modification of the sensor’s carrier concentration. On one hand, cleaned graphene shows little or no response to analytes such as

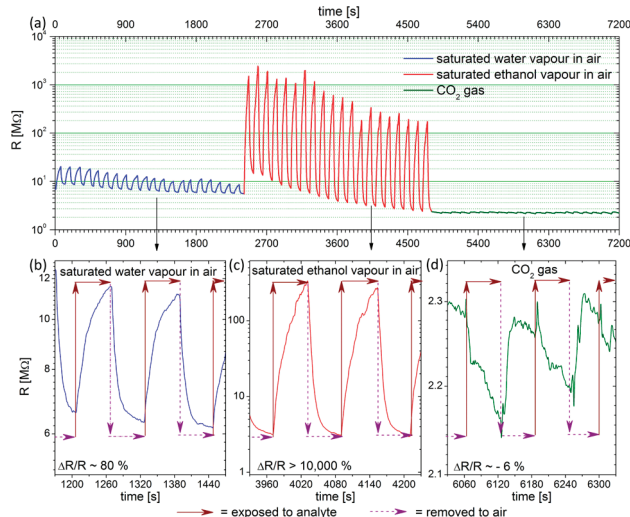


FIGURE 5. (a) Response of the electrical resistance R to the presence of water and ethanol vapor, and CO_2 gas, into which the sensor is periodically introduced and then removed to air. Note that the ordinate is plotted in logarithmic scale due to the extremely large response in ethanol. (b–d) Expanded regions from representative areas of the data in (a), with the response sensitivity $\Delta R/R$ indicated in each case. The significantly large response to ethanol vapor in the presence of air, water, and CO_2 makes this ideal for conductometric “breathalyzers” or industrial leakage sensors.

water vapor,²⁶ while on the other hand, covalent functionalization of multiwall carbon nanotubes with $-\text{COOH}$ groups significantly improves their sensitivity to water and ethanol vapor due to enhanced hydrogen bonding between the $-\text{OH}$ of the analytes and the $-\text{COOH}$ groups of the functionalized nanotubes.³² Owing to its strong affinity toward amphiphilic molecules, our PCA-functionalized graphene membrane have inbuilt sensitivity toward alcohol molecules. Indeed, conductometric sensing of various analyte vapors revealed that our sensor showed a large response to the presence of alcohols. Owing to its immediate relevance for breathalyzers and industrial alcohol leakage sensing, our experiments were performed in air (i.e., not in vacuum or in the presence of neutral gases) and were compared to responses to the presence of moisture and CO_2 , which are the other two major analyte components that would be present as a background in sensing. Figure 5 shows the comparative responses of a graphene sensor when exposed to saturated water vapor ($\sim 3\% \text{ v/v}$), ethanol vapor ($\sim 7.5\% \text{ v/v}$), and pure CO_2 gas. While the relative change in resistance in the presence of water vapor and CO_2 was found to be approximately 80% and -6% respectively, exposure to the saturated ethanol vapor was found to be in excess of 10 000%. Although our current experimental facilities are inadequate for controlled injection and detection of extremely small concentrations of gas/vapor molecules, the specific selectivity of our sensors to alcohols is an extremely encouraging result, and our future works will attempt to address the limit of detection in these sensors, and attempt to engineer different functionalization groups for other target-specific analytes.

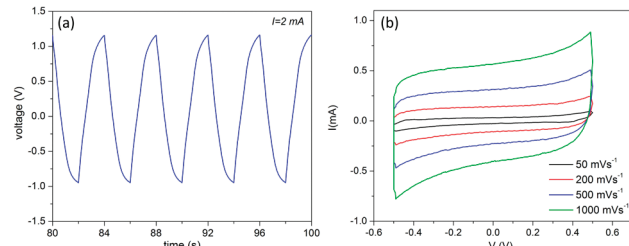


FIGURE 6. (a) Charge–discharge behavior of the graphene ultracapacitors performed at a constant current of 2 mA. The linear galvanostatic discharge confirms the capacitive behavior of the device. The slope of the discharge curve was used to calculate the value of specific capacitance. (b) Cyclic voltammograms (CV) obtained at various scan rates from EDLC electrodes fabricated with graphene flakes. The undistorted symmetric nature of the CV’s obtained at higher scan rate is indicative of fast charge transfer response of these electrodes.

Similar graphene-film membranes were used to fabricate ultrathin electrochemical double layer capacitors (EDLC),²⁵ or ultracapacitors. Ultracapacitors are high-energy storage devices with versatile applications ranging from high-pulse power backup operations to deep subvoltage nanoelectronics.³³ The high surface-to-volume ratio of carbon nanomaterials such as nanotubes and graphene enables extremely high specific charge storage. The performance of our ultracapacitors was characterized through galvanostatic charge–discharge measurements (Figure 6a) and cyclic voltammetry (Figure 6b) and were found to possess specific capacitance values as high as 120 F/g with impressive power densities ($\sim 105 \text{ kW/kg}$) and energy densities ($\sim 9.2 \text{ Wh/kg}$). In comparison, in capacitors fabricated from the parent graphite powder, the specific capacitance, maximum power density, and energy density were found to be orders of magnitude smaller in values. Operating without distortion at high scan rates up to 1000 mV/s (indicative of rapid charge transfer response of these electrodes) and even after 1000 charge–discharge cycles (data not shown) without the use of any binders or specially prepared current collectors, our ultracapacitors reflect a significant improvement over previously reported graphene-based ultracapacitors¹³ and are substantially better than those obtained with carbon nanotubes.³⁴

To conclude, we have presented a method for exfoliating graphene directly from graphite into aqueous dispersions using a noncovalent surface functionalization with PCA. In the past, PCA has been used to successfully debundle single wall carbon nanotubes¹⁹ that remain stably debundled despite their large size compared to individual PCA molecules. We believe that although PCA is a small molecule, large quantities of surface functionalization are helping achieve this debundling in case of nanotubes. A similar effect is not difficult to visualize in our case for graphene as well. We do note, however, that our exfoliated graphene flakes are a mixture of single and multilayer in nature, and our future research will attempt to improve the concentration of single-layer graphene flakes in the dispersion. One of the greatest advantages of our method is that it does not require

the chemical conversion of graphene. Although chemical conversion of graphene into graphene oxide (GO) enables formation of aqueous dispersions, GO is an insulator whose conducting properties can only be partially recovered when chemically converted to “reduced graphene oxide”. In our case, the solubility of graphene has been introduced by a noncovalent π -stacking mechanism that does not disrupt the sp^2 network of graphene. Our Raman studies confirm that the quality of the graphene produced is far superior compared to rGO, and quite similar to that produced via “micromechanical exfoliation”. Our method is inherently advantageous for large-scale applications development using high-quality graphene. It is devoid of any harsh chemicals or conditions such as strong acids or reducing agents, which are frequently adopted in other techniques for exfoliating graphene or developing dispersions of graphene oxide, or high-temperature annealing that may damage other system components. The absence of harsh chemicals becomes more meaningful for large-scale production where disposal of hazardous materials presents a significant additional complication. The starting material is graphite powder, which is an extremely low-cost material compared to highly oriented pyrolytic graphite (HOPG) used quite frequently as a starting material to produce graphene. The entire process is performed at room temperature, and hence is extremely friendly for a number of technologies where temperature limitations exist. In addition, Because of the low-temperature processing and low-energy consumption of the equipment required, the energy costs for production of large-scale quantities will be low. The process steps do not need any controlled environment chambers (e.g., CVD chambers or gas flow systems), enhancing its simplicity without compromising its scalability. This simplicity enables us to directly demonstrate high-performance applications related to environmental sensing and energy storage, which have become issues of global importance. Owing to these factors, in recent times there has been an increased effort to obtain graphene directly from graphite involving innovative exfoliation techniques such as surface energy engineering³⁵ in suitable organic solvents and surfactant-induced dispersion³⁶ into water-based media. In comparison to these works, our work represents a different method with a comparable yield of graphene in water and a marked absence of residual graphite flakes in dispersion. We believe that our method will be also useful for applications of graphene that require an aqueous medium, such as biomolecular experiments with living cells, or investigations involving glucose or protein interactions with graphene.

Acknowledgment. We gratefully acknowledge Dr. Huafang Li who helped us with HRTEM data acquisition. This work was supported by the Interconnect Focus Center New York at RPI, one of the five Focus Center Research Programs of Semiconductor Research Corporation. S.K. and S.T. acknowledge partial support by NSF ECCS 0925708 and NSF ECCS 0925682, respectively. S.T. also acknowledges funding

support provided by Office of Research and Development Administration at SIUC through Start-up funds and a seed grant.

Supporting Information Available. Detailed descriptions of the graphene exfoliation process, washing steps, characterization (including SEM, AFM, low-temperature transport, UV-vis spectrometry, Raman spectrometry, XPS data, HR-TEM and SAED data, fabrication of sensors and ultracapacitors, related discussions including calculations of specific capacitance, power and energy density, a list of advantages of our methods, and a table comparing our ultracapacitor performance with published and other available data are placed in the Supporting Information. This material is available free of charge via the Internet at <http://pubs.acs.org>.

REFERENCES AND NOTES

- (1) Novoselov, K. S.; Geim, A. K.; Morozov, S. V.; Jiang, D.; Katsnelson, M. I.; Grigorieva, I. V.; Dubonos, S. V.; Firsov, A. A. *Nature* **2005**, *438*, 197–200.
- (2) Katsnelson, M. I.; Novoselov, K. S.; Geim, A. K. *Nat. Phys.* **2006**, *2*, 620–625.
- (3) Pisana, S.; Lazzari, M.; Casiraghi, C.; Novoselov, K. S.; Geim, A. K.; Ferrari, A. C.; Mauri, F. *Nat. Mater.* **2007**, *6*, 198–201.
- (4) Nair, R. R.; Blake, P.; Grigorenko, A. N.; Novoselov, K. S.; Booth, T. J.; Stauber, T.; Peres, N. M. R.; Geim, A. K. *Science* **2008**, *320*, 1308–1308.
- (5) Schedin, F.; Geim, A. K.; Morozov, S. V.; Hill, E. W.; Blake, P.; Katsnelson, M. I.; Novoselov, K. S. *Nat. Mater.* **2007**, *6*, 652–655.
- (6) Novoselov, K. S.; Geim, A. K.; Morozov, S. V.; Jiang, D.; Zhang, Y.; Dubonos, S. V.; Grigorieva, I. V.; Firsov, A. A. *Science* **2004**, *306*, 666–669.
- (7) Novoselov, K. S.; Jiang, D.; Schedin, F.; Booth, T. J.; Khotkevich, V. V.; Morozov, S. V.; Geim, A. K. *Proc. Natl. Acad. Sci. U.S.A.* **2005**, *102*, 10451–10453.
- (8) Bolotin, K. I.; Sikes, K. J.; Jiang, Z.; Klima, M.; Fudenberg, G.; Hone, J.; Kim, P.; Stormer, H. L. *Solid State Commun.* **2008**, *146*, 351–355.
- (9) Lee, C.; Wei, X.; Kysar, J. W.; Hone, J. *Science* **2008**, *321*, 385–388.
- (10) Balandin, A. A.; Ghosh, S.; Bao, W.; Calizo, I.; Teweldebrhan, D.; Miao, F.; Lau, C. N. *Nano Lett.* **2008**, *8*, 902–907.
- (11) Eda, G.; Fanchini, G.; Chhowalla, M. *Nat. Nanotechnol.* **2008**, *3*, 270–274.
- (12) Fowler, J. D.; Allen, M. J.; Tung, V. C.; Yang, Y.; Kaner, R. B.; Weiller, B. H. *ACS Nano* **2009**, *3*, 301–306.
- (13) Stoller, M. D.; Park, S.; Zhu, Y.; An, J.; Ruoff, R. S. *Nano Lett.* **2008**, *8*, 3498–3502.
- (14) Park, S.; Ruoff, R. S. *Nat. Nanotechnol.* **2009**, *4*, 217–224.
- (15) Park, S.; An, J.; Jung, I.; Piner, R. D.; An, S. J.; Li, X.; Velamakanni, A.; Ruoff, R. S. *Nano Lett.* **2009**, *9*, 1593–1597.
- (16) Ferrari, A. C.; Meyer, J. C.; Scardaci, V.; Casiraghi, C.; Lazzari, M.; Mauri, F.; Piscanec, S.; Jiang, D.; Novoselov, K. S.; Roth, S.; Geim, A. K. *Phys. Rev. Lett.* **2006**, *97*, 187401-1–187401-4.
- (17) Graf, D.; Molitor, F.; Ensslin, K.; Stampfer, C.; Jungen, A.; Hierold, C.; Wirtz, L. *Nano Lett.* **2007**, *7*, 238–242.
- (18) Graf, D.; Molitor, F.; Ensslin, K.; Stampfer, C.; Jungen, A.; Hierold, C.; Wirtz, L. *Euro. Phys. J. Spec. Top.* **2007**, *148*, 171–176.
- (19) Simmons, T. J.; Bult, J.; Hashim, D. P.; Linhardt, R. J.; Ajayan, P. M. *ACS Nano* **2009**, *3*, 865–870.
- (20) Liu, J.; Rinzler, A. G.; Dai, H.; Hafner, J. H.; Bradley, R. K.; Boul, P. J.; Lu, A.; Iverson, T.; Shelimov, K.; Huffman, C. B.; Rodriguez-Macias, F.; Shon, Y. S.; Lee, T. R.; Colbert, D. T.; Smalley, R. E. *Science* **1998**, *280*, 1253–1256.
- (21) Fan, Z.; Wei, T.; Luo, G.; Wei, F. *J. Mater. Sci.* **2005**, *40*, 5075–5077.
- (22) Rosca, I. D.; Watari, F.; Uo, M.; Akasaka, T. *Carbon* **2005**, *43*, 3124–3131.

- (23) Marshall, M. W.; Popa-Nita, S.; Shapter, J. G. *Carbon* **2006**, *44*, 1137–1141.
- (24) Mawhinney, D. B.; Naumenko, V.; Kuznetsova, A.; Yates, J. T., Jr.; Liu, J.; Smalley, R. E. *Chem. Phys. Lett.* **2000**, *324*, 213–216.
- (25) Details available in the Supporting Information.
- (26) Dan, Y.; Lu, Y.; Kybert, N. J.; Luo, Z.; Johnson, A. T. C. *Nano Lett.* **2009**, *9*, 1472–1475.
- (27) *Handbook of Chemistry & Physics Online*, <http://www.hbcpnetbase.com/> Accessed July 6, 2009.
- (28) Thiele, H. Z. *Anorg. Und Allg. Chem.* **1932**, *206*, 407.
- (29) Hummers, W. S. U.S. Patent 2,798,878, 1957.
- (30) Hummers, W. S.; Offeman, R. E. *J. Am. Chem. Soc.* **1958**, *80*, 1339.
- (31) McKay, S. F. *J. Appl. Phys.* **1964**, *35*, 1992.
- (32) Sin, M. L. Y.; Chow, G. C. T.; Wong, G. M. K.; Li, W. J.; Leong, P. H. W.; Wong, K. W. *IEEE Trans. Nanotechnol.* **2007**, *6*, 571–577. (2007).
- (33) Despotuli, A.; Andreeva, A. *Modern Electronics* **2007**, *7*, 24–29, English: http://www.nanometer.ru/2007/10/17/nanoionnie_superkondensatori_4879/PROP_FILE_files_2/Despotuli_Andreeva_Modern_Electronics_2007_rus_eng_translation_4.pdf.
- (34) Talapatra, S.; Kar, S.; Pal, S. K.; Vajtai, R.; Ci, L.; Victor, P.; Shaijumon, M. M.; Kaur, S.; Nalamasu, O.; Ajayan, P. M. *Nat. Nanotechnol.* **2006**, *1*, 112–116.
- (35) Hernandez, Y.; et al. *Nat. Nanotechnol.* **2008**, *3*, 563–568.
- (36) Lotya, M.; et al. *J. Am. Chem. Soc.* **2009**, *131*, 3611–3620.